Transonic accretion flow in Cygnus X-1

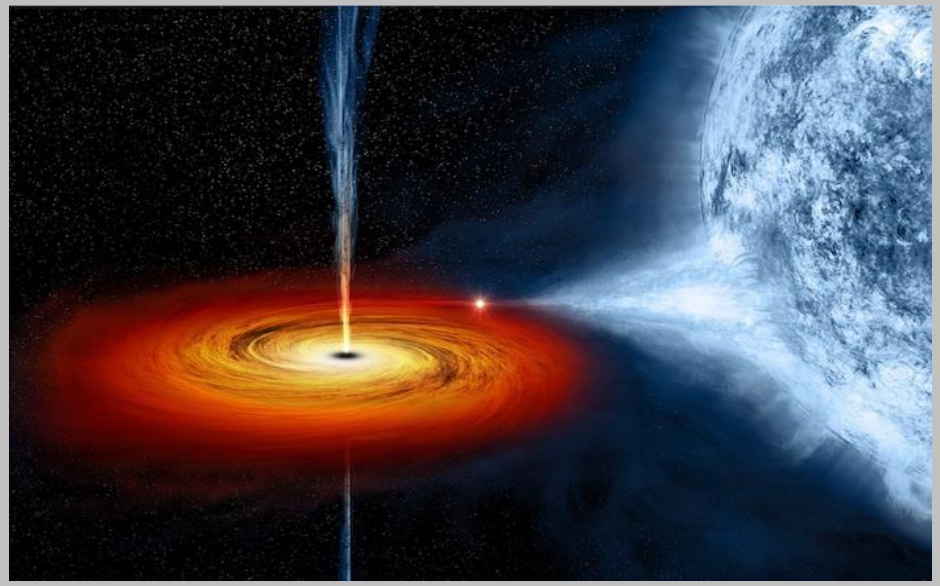

-Ishika Palit

Supervisor : Prof. Agnieszka Janiuk

Date : 24.09.2020

Virtual Conference of the Polish Society on Relativity 2020

Plan of Talk

- **Introduction to X-ray binaries**
- **Wind fed accretion in Cygnus X-1**
- **GRMHD simulation (HARM)**
- **Results and outcomes**

X-ray Binaries

X-ray Binary systems contain one normal star and one collapsed star that orbit around their common center of mass.

(low-mass X-ray binaries, LMXBs)

(high-mass X-ray binaries, HMXBs)

The X-rays are produced as material from the companion star is drawn to the compact object either through

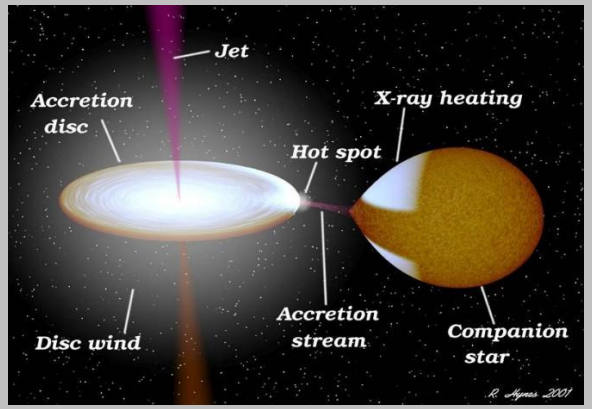

- Roche-lobe overflow into an accretion disk
- Direct impact of a stellar wind onto the compact object

Scorpius X-1 and Cygnus X-1 were first X-ray sources to be discovered in the constellations of Scorpius and Cygnus respectively.
HMXBs are brighter in X-rays not just because of accretion disk but also due to presence of extremely hot corona.

[credits- NASA/R. Hynes]

HMXB's

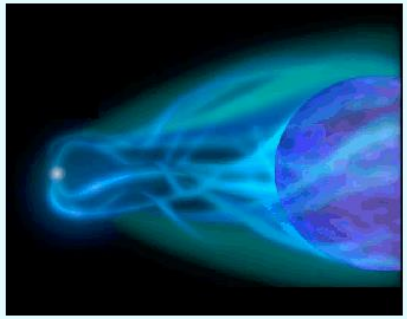

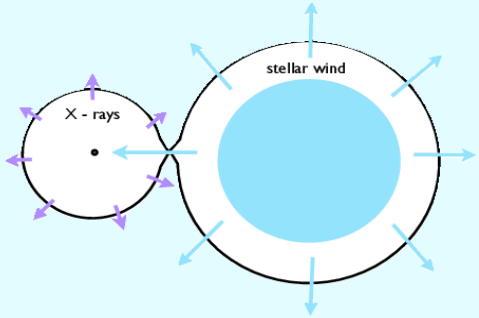

- High Mass companion star (≥10 M_0), mostly O or B type stars
- Mostly Stellar wind accretion
- If collapsed star less massive than companion then remains as a binary system.
- Higher energy X-ray emission.

LMXB's

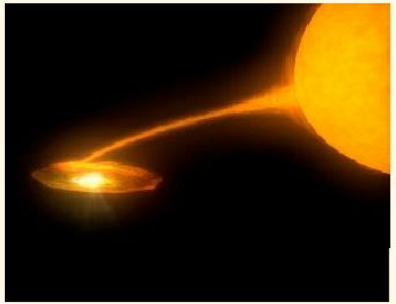

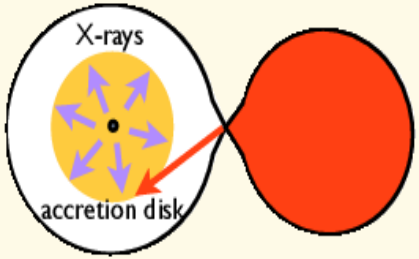

- Low Mass companion star (≤ 1M_0), mostly K or M type star or a white dwarf
- Roche Lobe overflow
- The mass transfer on to the compact object is much slower and more controlled.
- They emit lower energy X-rays.

Cygnus X-1: Spectra & wind properties

X-ray binary system:
Cygnus X-1 – Black hole ~ (20 M_o)
HDE-226868 – Supergiant star (~ 40 M_o)

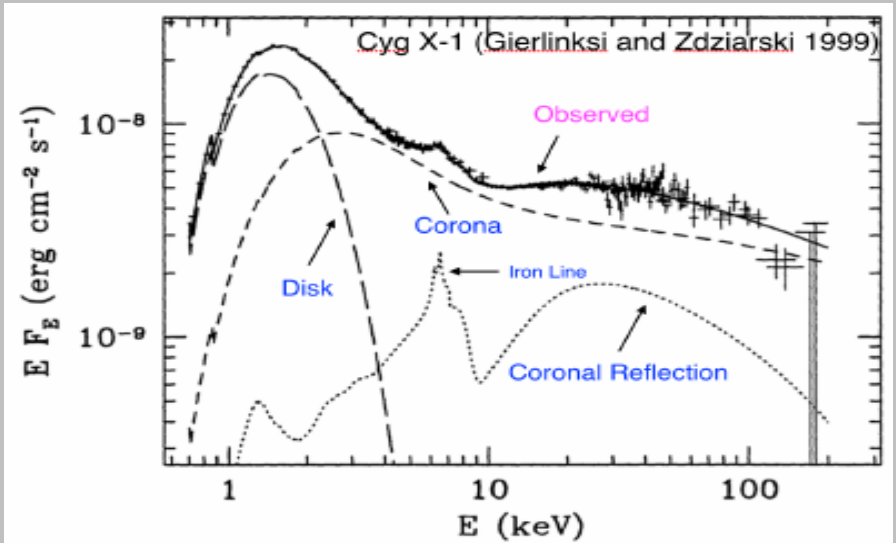

Focused stellar wind:

- Important variability component due to the variable (clumpy) stellar wind from the companion.
- Winds are powered by radiation pressure acting through absorption in spectral lines (CAK mechanism).
- Perturbations present in the wind causing variations in the parameters of the flow such as density, velocity and temperature, which compress the gas into small, cold, and over-dense structures, often referred to as “clumps”.
- These clumps are stated responsible for the observed absorption dips (i.e the lower flux) in the Hard State spectra

Cygnus X-1: Spectra & wind properties

X-ray binary system:
Cygnus X-1 – Black hole ~ (20 M_o)
HDE-226868 – Supergiant star (~ 40 M_o)

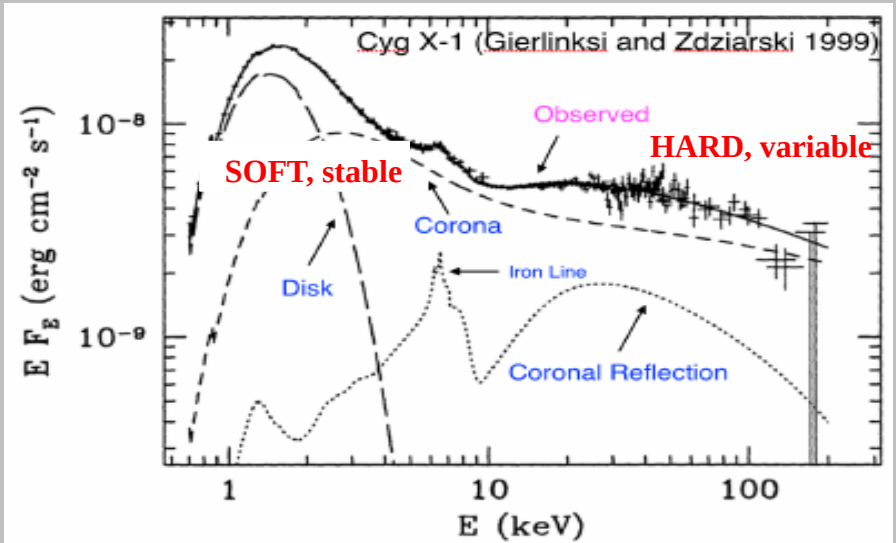

Focused stellar wind:

- Important variability component due to the variable (clumpy) stellar wind from the companion.
- Winds are powered by radiation pressure acting through absorption in spectral lines (CAK mechanism).
- Perturbations present in the wind causing variations in the parameters of the flow such as density, velocity and temperature, which compress the gas into small, cold, and over-dense structures, often referred to as “clumps”.
- These clumps are stated responsible for the observed absorption dips (i.e the lower flux) in the Hard State spectra

Cygnus X-1: Spectra & wind properties

X-ray binary system:
Cygnus X-1 – Black hole ~ (20 M_o)
HDE-226868 – Supergiant star (~ 40 M_o)

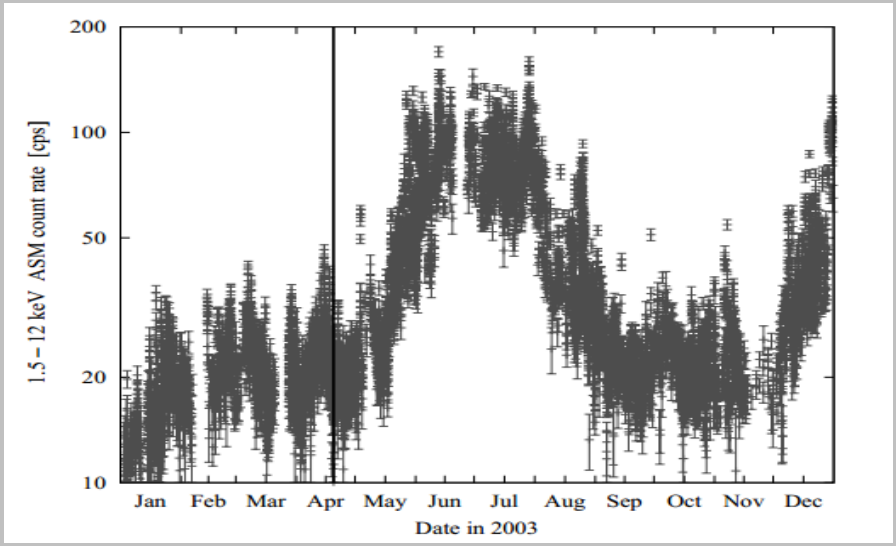

Focused stellar wind:

- Important variability component due to the variable (clumpy) stellar wind from the companion.
- Winds are powered by radiation pressure acting through absorption in spectral lines (CAK mechanism).
- Perturbations present in the wind causing variations in the parameters of the flow such as density, velocity and temperature, which compress the gas into small, cold, and over-dense structures, often referred to as “clumps”.
- These clumps are stated responsible for the observed absorption dips (i.e the lower flux) in the Hard State spectra

(Hanke, M. et. al , 2009, ApJ)

Cygnus X-1: Spectra & wind properties

X-ray binary system:
Cygnus X-1 – Black hole ~ (20 M_o)
HDE-226868 – Supergiant star (~ 40 M_o)

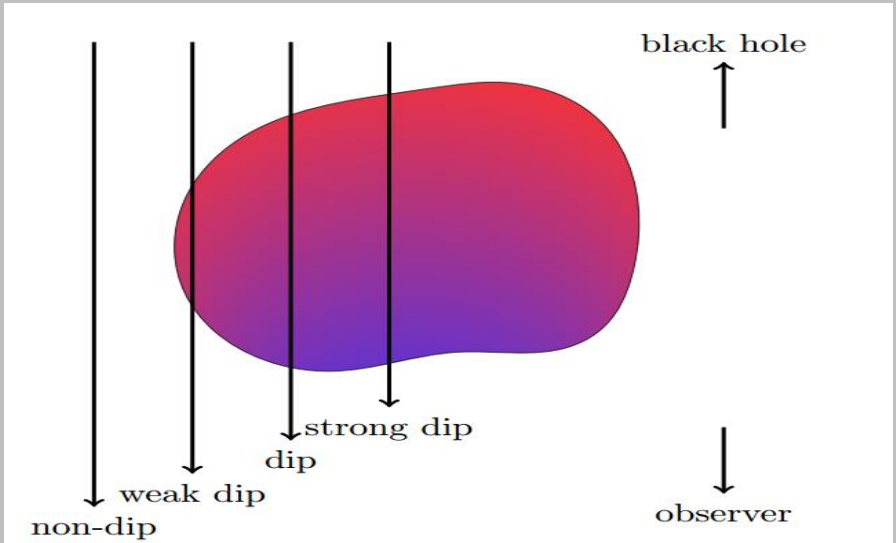

Focused stellar wind:

- Important variability component due to the variable (clumpy) stellar wind from the companion.
- Winds are powered by radiation pressure acting through absorption in spectral lines (CAK mechanism).
- Perturbations present in the wind causing variations in the parameters of the flow such as density, velocity and temperature, which compress the gas into small, cold, and over-dense structures, often referred to as “clumps”.
- These clumps are stated responsible for the observed absorption dips (i.e the lower flux) in the Hard State spectra

(Hirsch, M. et. al , 2019, A&A)

Cygnus X-1: Spectra & wind properties

X-ray binary system:
Cygnus X-1 – Black hole ~ (20 M_o)
HDE-226868 – Supergiant star (~ 40 M_o)

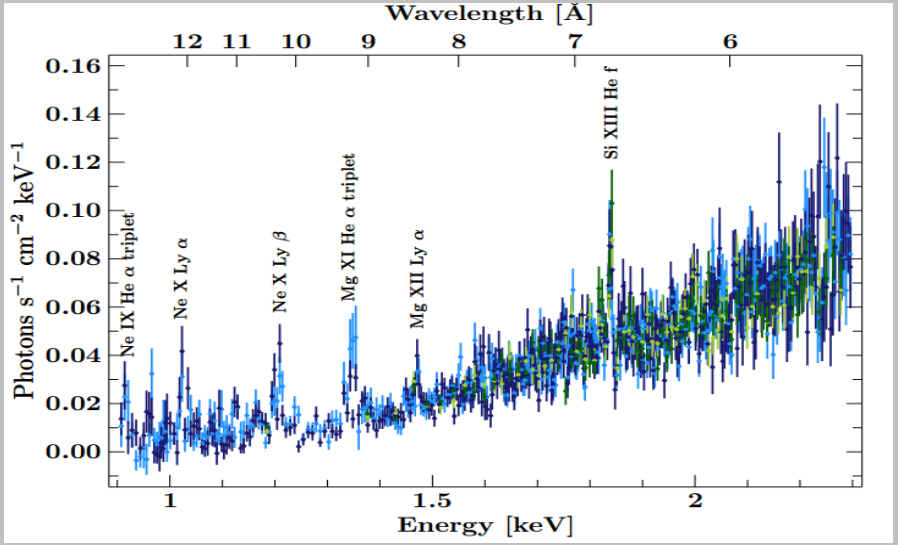

Focused stellar wind:

- Important variability component due to the variable (clumpy) stellar wind from the companion.
- Winds are powered by radiation pressure acting through absorption in spectral lines (CAK mechanism).
- Perturbations present in the wind causing variations in the parameters of the flow such as density, velocity and temperature, which compress the gas into small, cold, and over-dense structures, often referred to as “clumps”.
- These clumps are stated responsible for the observed absorption dips (i.e the lower flux) in the Hard State spectra

(Hirsch, M. et. al , 2019, A&A)

Our model set-up

- **The prescription of density at the outer boundary is estimated from the observed data [$\rho_{max} = 10^{-15}$ g cm^{-3} (15000 [M]) , $\rho_{min} = 0$ g cm^{-3}]**
- **The choice for angular momentum is motivated by the values of angular momentum at marginally stable orbit, $\lambda_{ms} = 3.67\ GM_{BH}/c^2$ and at marginally bound orbit, $\lambda_{mb} = 4GM_{BH}/c^2$** (Das & Chakrabarti 1999).
- **We implement a function generating values between the prescribed maximum and minimum amplitude of density & angular momentum.**

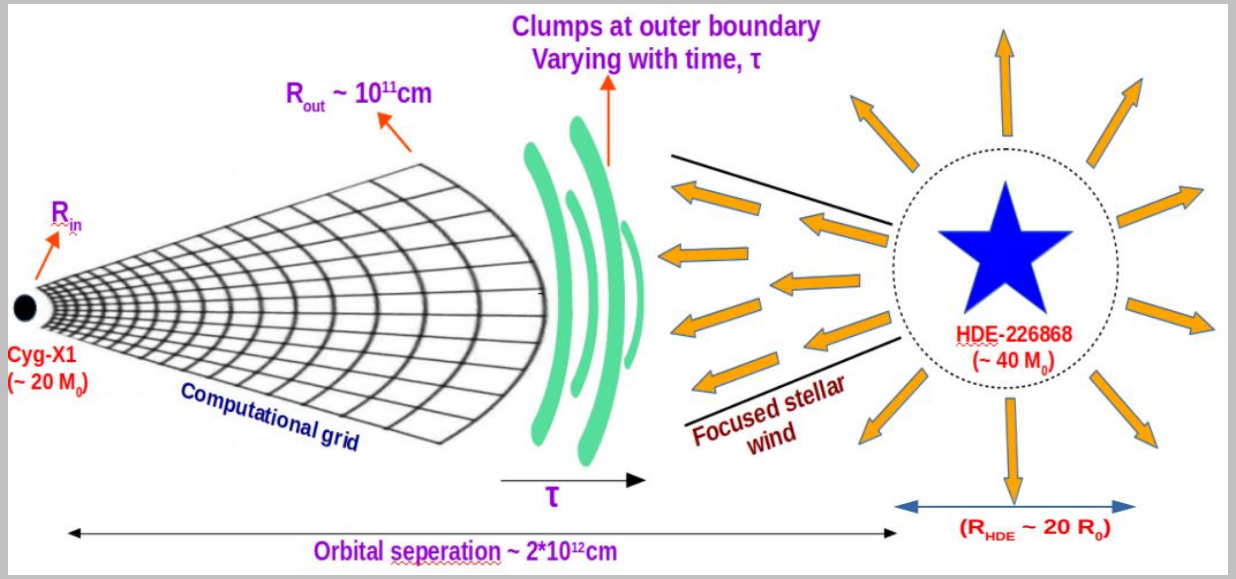

(Ref: I.Palit et.al, 2020, ApJ)

Our model set-up

- **The prescription of density at the outer boundary is estimated from the observed data [$\rho_{max} = 10^{-15}$ g cm^{-3} (15000 [M]) , $\rho_{min} = 0$ g cm^{-3}]**

- **The choice for angular momentum is motivated by the values of angular momentum at marginally stable orbit, $\lambda_{ms} = 3.67\ GM_{BH}/c^2$ and at marginally bound orbit, $\lambda_{mb} = 4GM_{BH}/c^2$** (Das & Chakrabarti 1999).

- **We implement a function generating values between the prescribed maximum and minimum amplitude of density & angular momentum.**

Angular Momentum

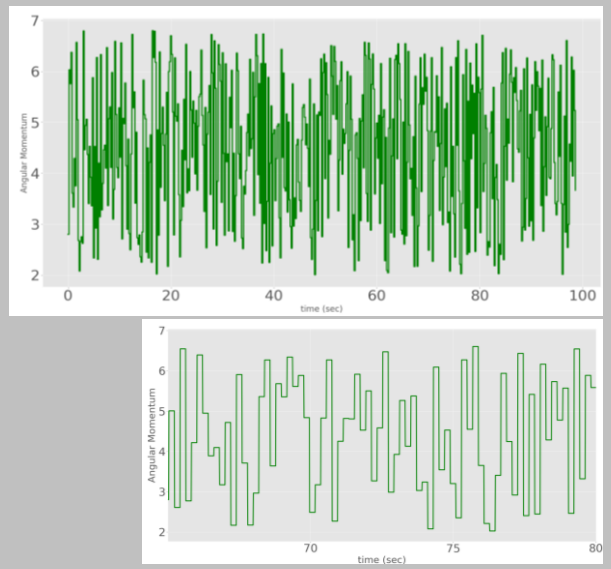

Density

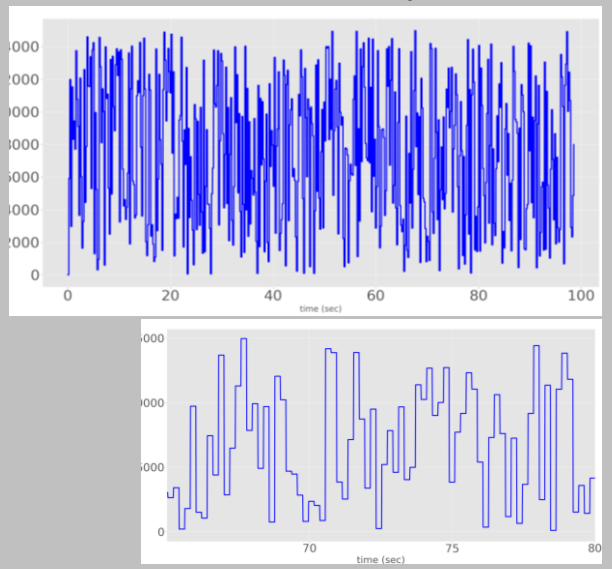

($\lambda_{max} = 2.0$[M] , $\lambda_{min} = 6.8$ [M])

(Ref: I.Palit et.al, 2020, ApJ)

Initial conditions & shock solution

Initial conditions:

- **Quasi-spherical distribution of gas, provided by constant specific angular momentum for a non-Keplerian accretion disk.**
  (Abramowicz & Zurek 1981)
- **Transonic Accretion - Shock solution (Pressure waves travel with sound speed) , C_{sound} = (Pressure * adiabatic index)/ density**
- **Time dependent outer boundary condition**
- **Inviscid, non-magnetized flow**
- **Polytropic Equation of state ($P = K\rho^{\gamma}$)**

Initial conditions & shock solution

Initial conditions:

- **Quasi-spherical distribution of gas, provided by constant specific angular momentum for a non-Keplerian accretion disk.** (Abramowicz & Zurek 1981)
- **Transonic Accretion - Shock solution (Pressure waves travel with sound speed) , C_{sound} = (Pressure * adiabatic index)/ density**
- **Time dependent outer boundary condition**
- **Inviscid, non-magnetized flow**
- **Polytropic Equation of state ($P = K\rho^{\gamma}$)**

Shock solution:

$$\dot{M} = u \rho r^2$$

Mass conservation equation

$$u\frac{du}{dr} + \frac{1}{\rho}\frac{dP}{dr} + \frac{d}{dr}(\Phi(r)) = 0$$

radial momentum equation

$$\epsilon = \frac{1}{2}u^2 + \frac{a^2}{(\gamma - 1)} + \frac{\lambda^2}{2}r^2 + \phi = 0$$

energy conservation equation in steady state

Initial conditions & shock solution

Initial conditions:

- **Quasi-spherical distribution of gas, provided by constant specific angular momentum for a non-Keplerian accretion disk.** (Abramowicz & Zurek 1981)
- **Transonic Accretion - Shock solution (Pressure waves travel with sound speed) , C_{sound} = (Pressure * adiabatic index)/ density**
- **Time dependent outer boundary condition**
- **Inviscid, non-magnetized flow**
- **Polytropic Equation of state ($P = K\rho^{\gamma}$)**

Shock solution:

$$a_c = \sqrt{\frac{r}{2}\frac{d\phi(r)}{dr} - \frac{\lambda^2}{2r^2}} = \sqrt{\frac{r}{4(r-1)^2} - \frac{\lambda^2}{2r^2}}$$

local sound speed

$$\epsilon = \frac{1}{2}u^2 + \frac{a^2}{(\gamma-1)} + \frac{\lambda^2}{2}r^2 + \phi = 0$$

energy conservation equation in steady state

Initial conditions & shock solution

Initial conditions:

- **Quasi-spherical distribution of gas, provided by constant specific angular momentum for a non-Keplerian accretion disk.** (Abramowicz & Zurek 1981)
- **Transonic Accretion - Shock solution (Pressure waves travel with sound speed) , C_{sound} = (Pressure * adiabatic index)/ density**
- **Time dependent outer boundary condition**
- **Inviscid, non-magnetized flow**
- **Polytropic Equation of state ($P = K\rho^{\gamma}$)**

Shock solution:

Critical point, r_c $(\varepsilon,\lambda,\gamma)$:

$$\epsilon - \frac{\lambda^2}{2r_c^2} - \frac{\gamma+1}{2(\gamma-1)}\left(\frac{r_c}{4(r_c-1)^2} - \frac{\lambda^2}{2r_c^2}\right) = 0$$

Mach Number ($\mathcal{M}$) = $\frac{\text{Flow Velocity}}{\text{Local sound speed}}$

(Suková P. et.al, 2015, MNRAS)
(Suková P. et.al, 2017, MNRAS)
(Palit, I. et.al, 2019, MNRAS)

Initial conditions & shock solution

Initial conditions:

- **Quasi-spherical distribution of gas, provided by constant specific angular momentum for a non-Keplerian accretion disk.** (Abramowicz & Zurek 1981)
- **Transonic Accretion - Shock solution (Pressure waves travel with sound speed) , C_{sound} = (Pressure * adiabatic index)/ density**
- **Time dependent outer boundary condition**
- **Inviscid, non-magnetized flow**
- **Polytropic Equation of state ($P = K\rho^{\gamma}$)**

Shock solution:

Critical point, r_c ($\varepsilon,\lambda,\gamma$):

$$\epsilon - \frac{\lambda^2}{2r_c^2} - \frac{\gamma+1}{2(\gamma-1)}\left(\frac{r_c}{4(r_c-1)^2} - \frac{\lambda^2}{2r_c^2}\right) = 0$$

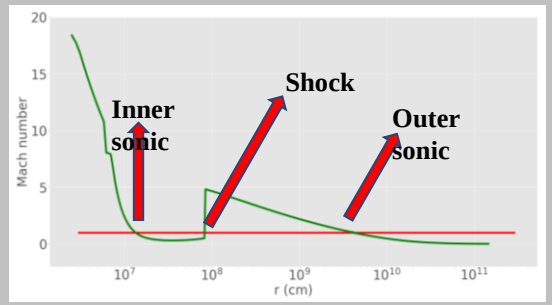

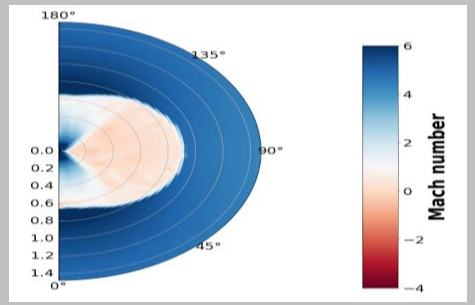

Mach Number ($\mathcal{M}$) = Flow Velocity / Local sound speed

(Suková P. et.al, 2015, MNRAS)
(Suková P. et.al, 2017, MNRAS)
(Palit, I. et.al, 2019, MNRAS)

Subsonic ($\mathcal{M} < 1$), Supersonic($\mathcal{M} > 1$)

HARM
(High Accuracy Relativistic magnetohydrodynamic)

HARM is a conservative shock capturing scheme, for evolving the equations of GRMHD
(developed by C.Gammie et al. 2003)

(Current version of code have many modifications and additions by Prof. Janiuk and group)

Continuity eq :

$$\frac{1}{\sqrt{-g}}\partial_\mu(\sqrt{-g}\ \rho u^\mu) = 0,$$

Four-momentum-energy conservation eq:

$$\partial_t(\sqrt{-g}\ T^t_{\ \nu}) = -\partial_i(\sqrt{-g}\ T^i_{\ \nu}) + \sqrt{-g}\ T^\kappa_{\ \lambda}\Gamma^\lambda_{\ \nu\kappa},$$

Induction eq:

$$\partial_t(\sqrt{-g}\ B^i) = -\partial_j(\sqrt{-g}\ (b^j u^i - b^i u^j)).$$

Stress tensor separates into gas and electromagnetic parts:

$$T^{\mu\nu} = T^{\mu\nu}_{gas} + T^{\mu\nu}_{EM},$$
$$T^{\mu\nu}_{gas} = \rho h u^\mu u^\nu + p g^{\mu\nu} = (\rho + u + p)u^\mu u^\nu + p g^{\mu\nu},$$
$$T^{\mu\nu}_{EM} = b^2 u^\mu u^\nu + \frac{1}{2} b^2 g^{\mu\nu} - b^\mu b^\nu; b^\mu = u^*_\nu F^{\mu\nu}.$$

HARM
(High Accuracy Relativistic magnetohydrodynamic)

HARM is a conservative shock capturing scheme, for evolving the equations of GRMHD
(developed by C.Gammie et al. 2003)

(Current version of code have many modifications and additions by Prof. Janiuk and group)

(GRMHD)

Continuity eq :

$$\frac{1}{\sqrt{-g}}\partial_\mu(\sqrt{-g}\ \rho u^\mu) = 0,$$

Four-momentum-energy conservation eq:

$$\partial_t(\sqrt{-g}\ T^t{}_\nu) = -\partial_i(\sqrt{-g}\ T^i{}_\nu) + \sqrt{-g}\ T^\kappa_\lambda \Gamma^\lambda{}_{\nu\kappa},$$

Induction eq:

$$\partial_t(\sqrt{-g}\ B^i) = -\partial_j(\sqrt{-g}\ (b^j u^i - b^i u^j)).$$

Stress tensor separates into gas and electromagnetic parts:

$$T^{\mu\nu} = T^{\mu\nu}_{gas} + T^{\mu\nu}_{EM},$$
$$T^{\mu\nu}_{gas} = \rho h u^\mu u^\nu + p g^{\mu\nu} = (\rho + u + p) u^\mu u^\nu + p g^{\mu\nu},$$
$$T^{\mu\nu}_{EM} = b^2 u^\mu u^\nu + \frac{1}{2} b^2 g^{\mu\nu} - b^\mu b^\nu, \quad b^\mu = u_\nu {}^*F^{\mu\nu}$$

Numerical Scheme:

- 2-D simulations are axisymmetric, i.e.the derivatives of quantities in φ-direction are neglected (however, velocity field and magnetic field vectors still have all the 3 components)

- HARM solves GRMHD equations in modified version of Kerr-Schild coordinate system (KS) rather than Boyer-Lindquist coordinates.

- The integrated equations are of the form: $$\partial_t \boldsymbol{U}(\boldsymbol{P}) = -\partial_i \boldsymbol{F}^i(\boldsymbol{P}) + \boldsymbol{S}(\boldsymbol{P}),$$

- **Choices added for outer boundary conditions:**
  - **1] Bound – Default** (No mass inflow or outflow)
  - **2] Bound - Fixed** (I. Palit et.al, 2019)
  - **3] Bound - Time** (I. Palit et.al, 2020)

Results: Effects due to time dependent outer boundary conditions

Angular Momentum

Density

Mach number

Radial Velocity

Results: Effects due to time dependent outer boundary conditions

Angular Momentum

Density

Mach number

Radial Velocity

Angular momentum profile close to Horizon

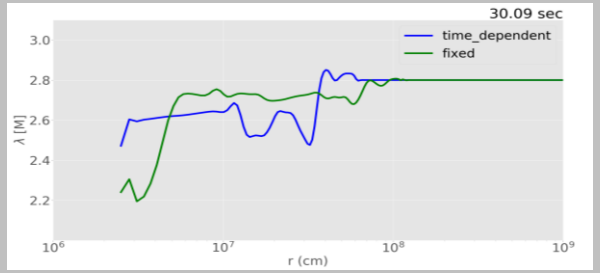

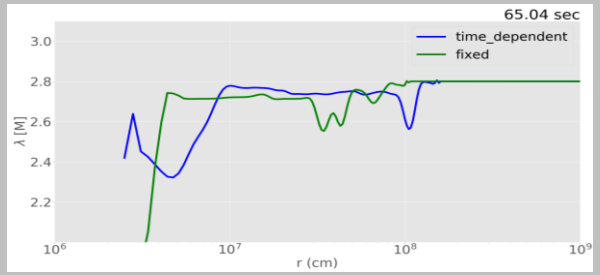

Results: 2D snapshots and Shock evolution

Mach Number

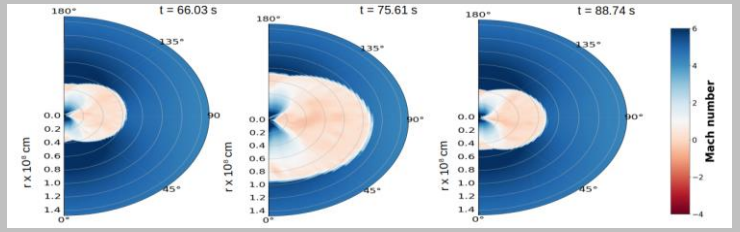

Density

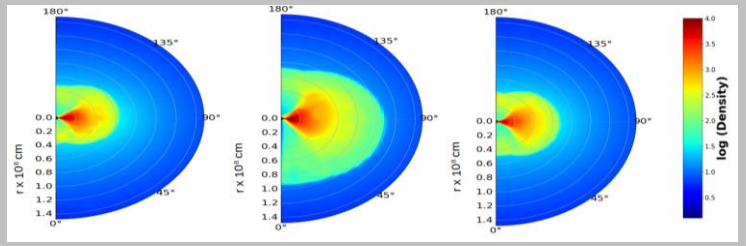

Angular Momentum

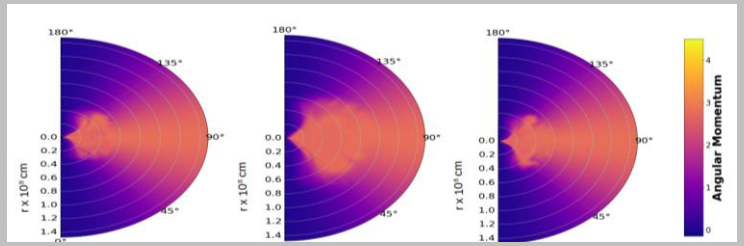

Shock evolution

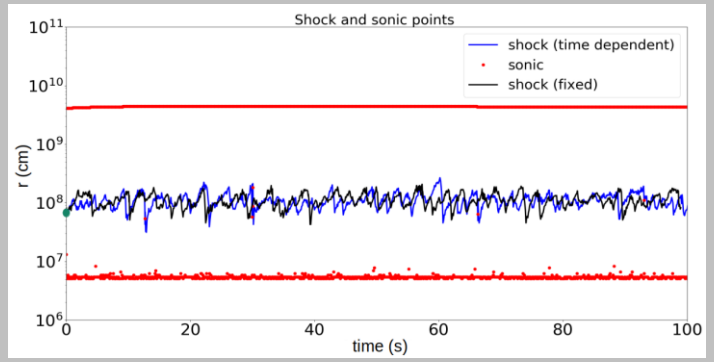

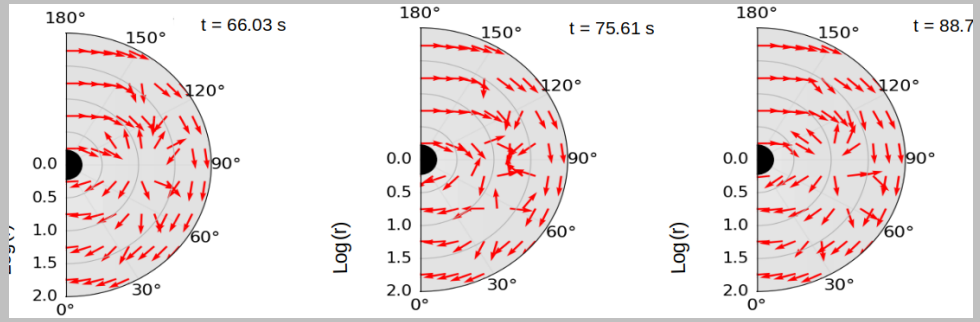

Velocity field lines

Results: Mass accretion rate & Power Density Spectra (PDS)

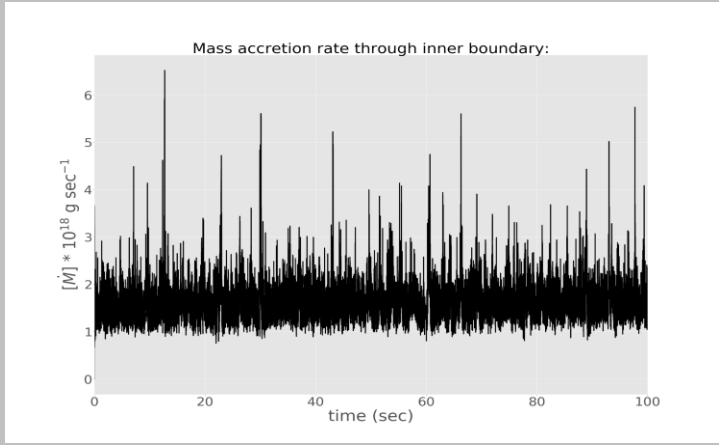

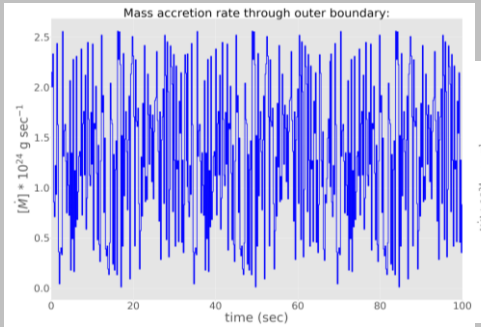

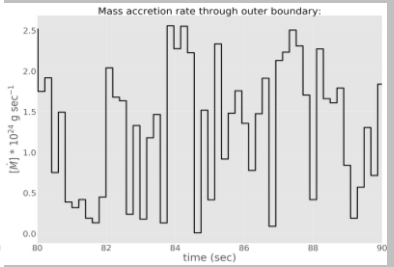

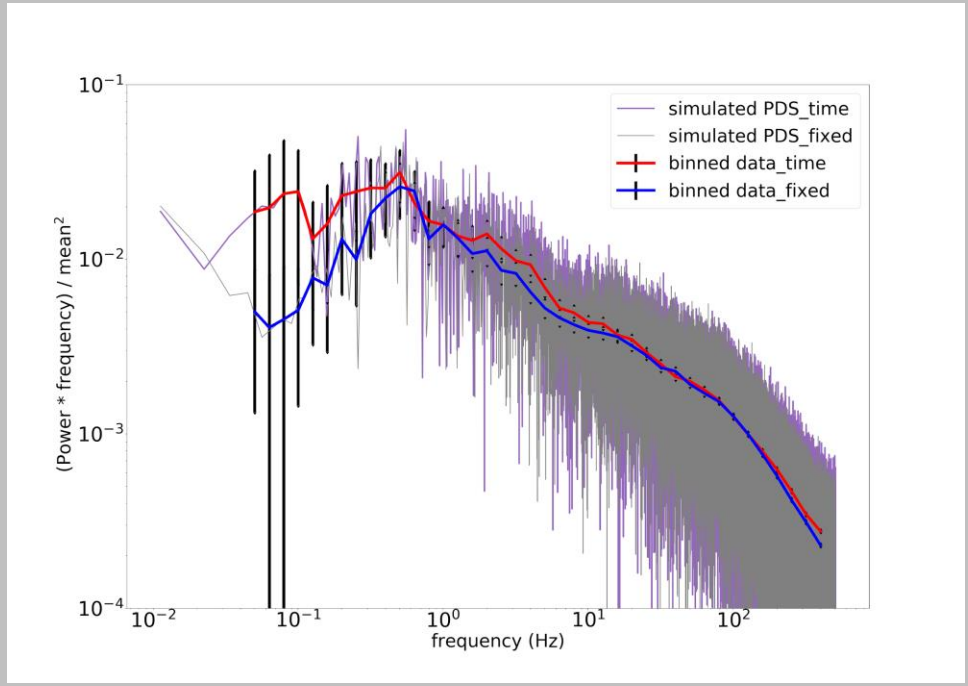

Comparison to observational Data

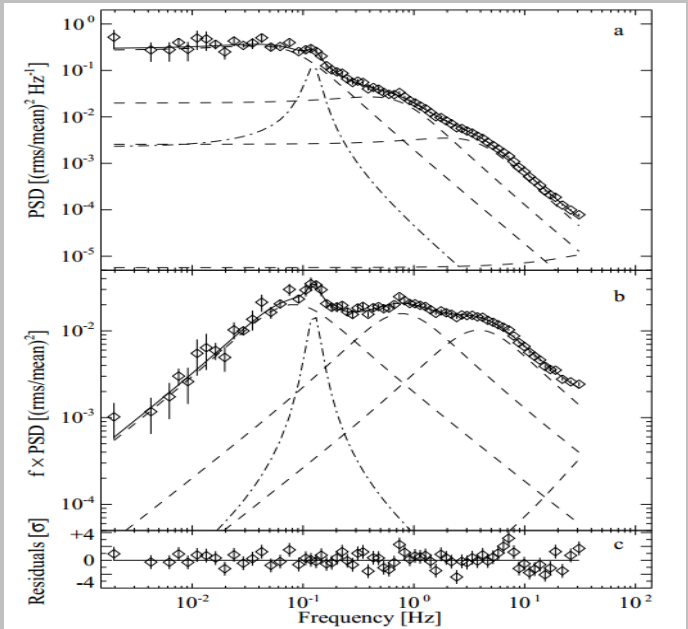

Fig. 2. a–c) Another typical fit, in this case to one of the P30157 observations (No. 11, 1998 February 20) in the 0.002–32 Hz frequency range. The best fit consists of four broad and one narrow Lorentzian profiles.

Pottschmidt et al. (2003)

$$L(f) = \pi^{-1} \frac{2R^2 Q f_r}{f_r^2 + 4Q^2(f - f_r)^2}$$

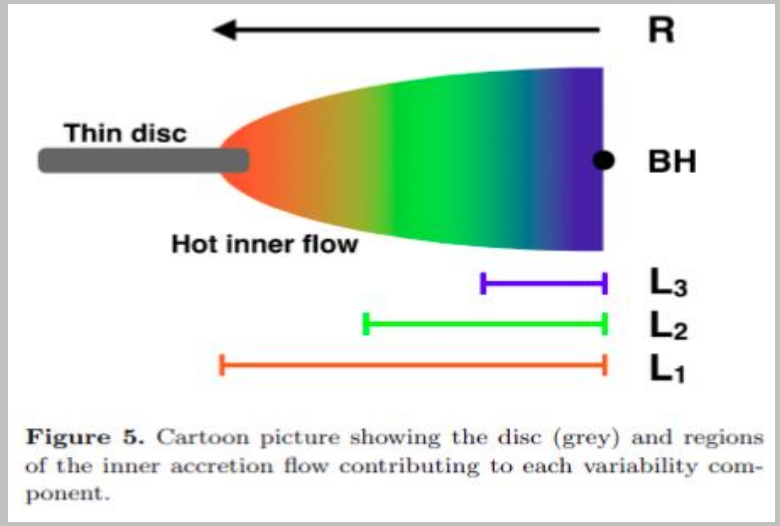

Figure 5. Cartoon picture showing the disc (grey) and regions of the inner accretion flow contributing to each variability component.

Axelsson & Done (2018)

Results: Lorentzian Fitting

Reduced χ^2 :

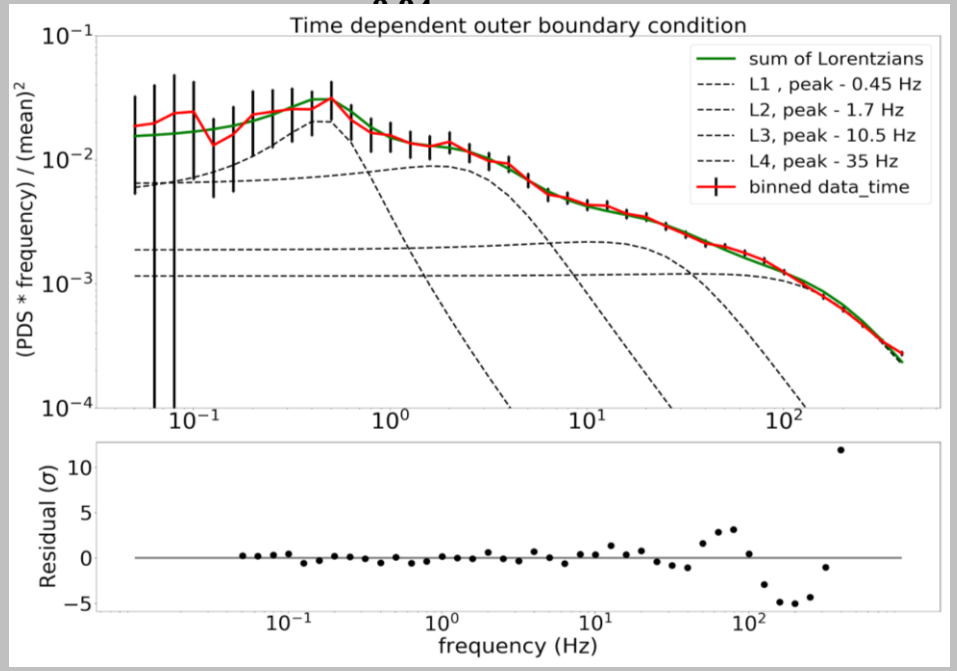

Reduced χ^2 : 15.25

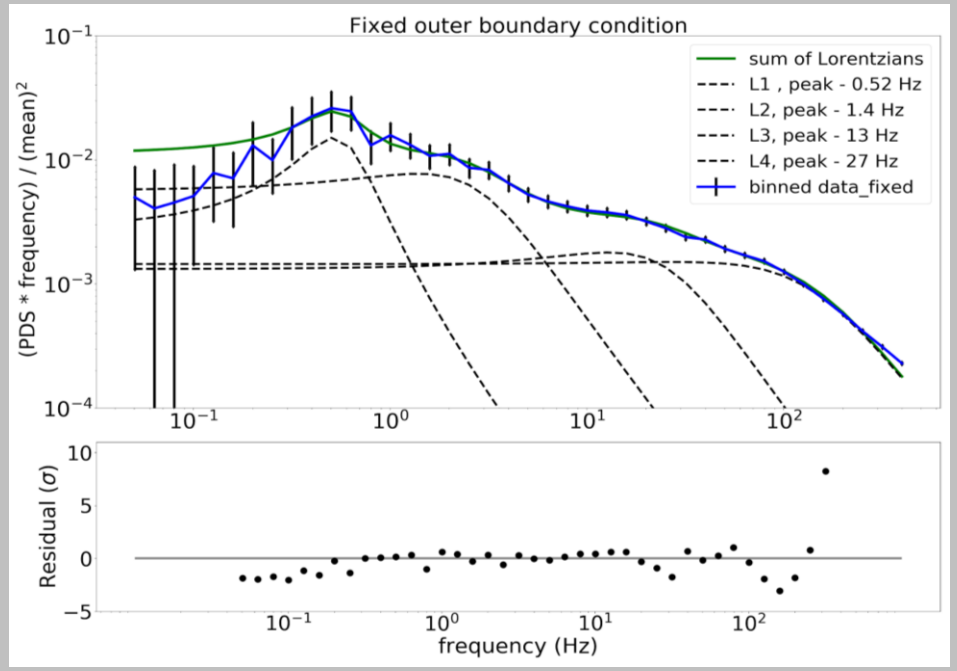

Comparison to observational Data

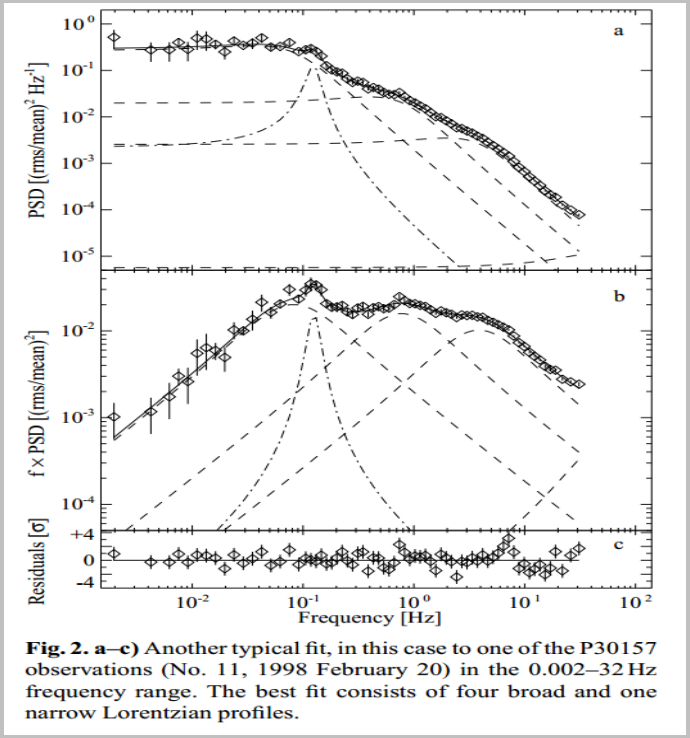

Fig. 2. a–c) Another typical fit, in this case to one of the P30157 observations (No. 11, 1998 February 20) in the 0.002–32 Hz frequency range. The best fit consists of four broad and one narrow Lorentzian profiles.

Pottschmidt et al. (2003)

The corresponding peak frequencies from our time dependent model are: **0.45 Hz,1.7 Hz, 10.5 Hz, and 35.0 Hz.**

L4 40 Hz
L3 6.0 Hz
L2 2.0 Hz
L1 0.2 Hz

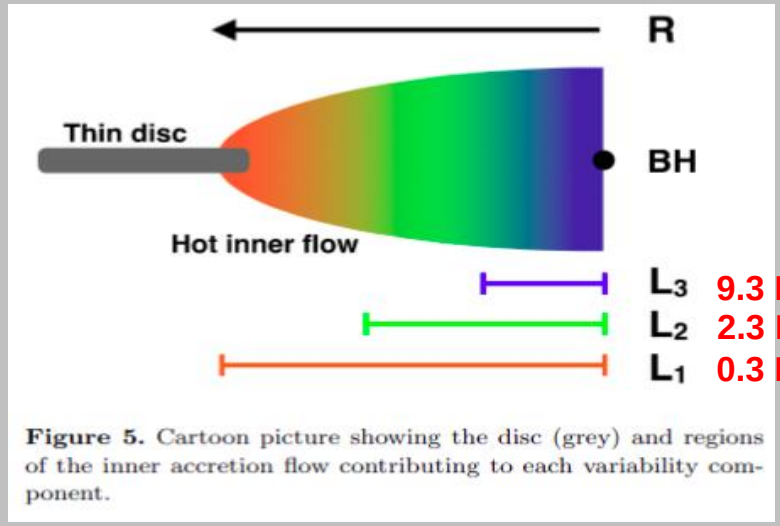

Figure 5. Cartoon picture showing the disc (grey) and regions of the inner accretion flow contributing to each variability component.

Axelsson & Done (2018)

Some comments on our outcome

- Our model cannot directly address the issue of the location of the specific emission component since the emissivity properties of the hot medium are not yet included in our model.

- On the other hand, we follow numerically the flow dynamics so all the aspects of the variability model based on the idea of the propagating fluctuations (Lyubarskii 1997; Kotov et al. 2001; Ingram & Done 2012) are automatically included by us.

- The model we use is appropriate for black hole accretion due to the specific inner boundary conditions.

- Our time-dependent evolution of the hot flow does not yet include the interaction with the cold disk which likely overlaps with the hot flow at some range of radii even in the Hard State (e.g. Basak et al. 2017; Zdziarski & De Marco 2020)

- Out of these all effects, the issue of the angular momentum budget is the most important one for our model since the existence of the shock requires the angular momentum removal to remain in the proper parameter space.

Conclusion

The Lorentzian fitting shows that the hot flow close to the black hole is mostly similar for models with and without wind but the major difference can be seen in the first Lorentzian which represents the oscillations at large radii.

The χ^2 values are high in our models due to very small statistical errors in the high frequency part in the PDS. They are actually dominated by the highest frequency point. Below 100 Hz the deviations in individual bins are of order of 2σ or smaller, very similar to the data residuals shown in Pottschmidt et al. (2003).

Our low-angular momentum coronal accretion model is able to represent the propagation of the perturbation from the outer boundary and explain the variability pattern seen in the Hard State of Cygnus X-1. arXiv:2009.09121